Biomech Model Mechanobiol
DOI 10.1007/s10237-015-0734-5

ORIGINAL PAPER

Multiscale evaluation of cellular adhesion alteration and cytoskeleton remodeling by magnetic bead twisting

Daniel Isabey[1] · **Gabriel Pelle**[1,2] · **Sofia André Dias**[1] · **Mathieu Bottier**[1] · **Ngoc-Minh Nguyen**[1] · **Marcel Filoche**[1,3] · **Bruno Louis**[1]

Received: 7 July 2015 / Accepted: 29 September 2015

Abstract Cellular adhesion forces depend on local biological conditions meaning that adhesion characterization must be performed while preserving cellular integrity. We presently postulate that magnetic bead twisting provides an appropriate stress, i.e., basically a clamp, for assessment in living cells of both cellular adhesion and mechanical properties of the cytoskeleton. A global dissociation rate obeying a Bell-type model was used to determine the natural dissociation rate (K_{off}^{0}) and a reference stress (σ_c). These adhesion parameters were determined in parallel to the mechanical properties for a variety of biological conditions in which either adhesion or cytoskeleton was selectively weakened or strengthened by changing successively ligand concentration, actin polymerization level (by treating with cytochalasin D), level of exerted stress (by increasing magnetic torque), and cell environment (by using rigid and soft 3D matrices). On the whole, this multiscale evaluation of the cellular and molecular responses to a controlled stress reveals an evolution which is consistent with stochastic multiple bond theories and with literature results obtained with other molecular techniques. Present results confirm the validity of the proposed bead-twisting approach for its capability to probe cellular and molecular responses in a variety of biological conditions.

Keywords Integrin-RGD binding · Dissociation rate · Multiple bonds · Clamp · Viscoelastic model

Electronic supplementary material The online version of this article (doi:10.1007/s10237-015-0734-5) contains supplementary material, which is available to authorized users.

For this research, we acknowledge receipt of grants from Agence Nationale de la Recherche: ANR no 2010-BLAN-1119-05 and from Fondation pour la Recherche Médicale: FRM programme Bio-Ingénierie pour la Santé 2014, DBS 201420140930771. Sofia André Dias is a PhD student supported by Agence Nationale de la Recherche et Technologies (ANRT) and Bertin Technologies, Mathieu Bottier is PhD student supported by INSIS CNRS 2013, Ngoc-Minh Nguyen is a postdoctoral student supported by ANR and FRM.

✉ Daniel Isabey
daniel.isabey@inserm.fr

Gabriel Pelle
gabriel.pelle@inserm.fr

Sofia André Dias
sofia.andre-dias@inserm.fr

Mathieu Bottier
mathieu.bottier@inserm.fr

Ngoc-Minh Nguyen
ngoc-minh.nguyen@inserm.fr

Marcel Filoche
marcel.filoche@polytechnique.edu

Bruno Louis
bruno.louis@inserm.fr

1 Introduction

Understanding cellular function at the molecular level is one the key challenges of modern biology. Whole cellular properties, e.g., shape, mechanical properties, as well as cellular response to chemical and mechanical cues, are all tightly cou-

[1] Inserm, U955, Équipe 13, Biomécanique & Appareil Respiratoire: une approche multi-échelle, UMR S955, CNRS, ERL 7240, Université Paris Est, UPEC, 8, rue du Général Sarrail, 94010 Créteil Cedex, France

[2] APHP, Groupe Hospitalier H. Mondor A. Chenevier, Service des Explorations Fonctionnelles 51, Avenue du Maréchal de Lattre de Tassigny, 94010 Créteil Cedex, France

[3] Physique de la Matière Condensée, Ecole Polytechnique, CNRS, 91128 Palaiseau, France

Published online: 12 October 2015

pled to and thus dependent on molecular mechanisms (Zhu et al. 2000). These molecular mechanisms develop (i) in the three-dimensional protein network called the cytoskeleton (CSK), giving rise to specific dynamic intracellular properties (in terms of adaptability, internal tension, stiffness, frequency response, remodeling), (ii) in the two-dimensional lipid bilayer which forms the membrane, i.e., a structure in constant interaction with extracellular matrix (ECM) and the neighboring cells. The bindings between major CSK filaments and the membrane appears essentially weak and transient (Janmey 1995). An appropriate model is to consider that cells assemble complexes of various proteins and primarily integrins at discrete points where the cytoskeleton attaches to the membrane, e.g., the focal adhesion sites in tissue cells (Burridge et al. 1988). These molecular complexes form a well-identified force-transmitting physical bridge which also acts as an effective force-sensing pathway. The cell respond to mechanical stress by molecular reinforcement through receptor–ligand binding, clustering, and active CSK rearrangement, through specific signaling pathways and effectors (Zhu et al. 2000). Hence, changing the number of bonds is an efficient way to control the strength of noncovalent bonds which are weak by nature and thus need to work together to resist force. Increasing bond number can be seen as a key mechanisms of reinforcement of weak noncovalent receptor–ligand bonds which is controlled by an active membrane-specific control of binding and clustering.

Nevertheless, single-molecule force spectroscopy experiments performed on the surface of living cells are unable to attain the ligand receptor stabilization mechanisms that occur within structured adhesion sites. One reason is that integrin clustering and focal adhesion maturation leading to the formation of parallel and multivalent ligand–receptor bonds may thereby deeply modify the effective lifetime of the integrin–ligand interactions (Schoen et al. 2013). Thus, there is a crucial need to investigate mechanical interactions of cells and their surrounding matrix in well-defined and realistic physiological conditions such as the in vitro culture conditions. This is a challenging problem because complex bond association needs to consider new influencing parameters such as the bond configuration or the bond number as done in the present approach. Moreover, measuring cell mechanical properties embedded in a 3D matrix constitutes another challenge since classical microscopic or micromanipulation techniques cannot be used.

To demonstrate that the classical magnetic bead-twisting cytometry method (MTC) initially invented by Wang et al. (1993) is capable to overcome these recurrent difficulties, we performed experiments with MTC in some emblematic epithelial cells exhibiting a phenotype similar to type II pneumocytes, (i.e., A549 cell lines), cultured them in different well-controlled physicochemical conditions susceptible to alter either adhesion or mechanical properties or both. These data are analyzed to estimate whether or not the method provides meaningful estimate of adhesion parameters and cell mechanical properties. Because the binding between intra- and extracellular mediums appears weak by nature, the cell response was partitioned between a pericellular binding behavior, i.e., the cellular adhesion, and an intracellular binding behavior, i.e., the cellular structure. The evolution of kinetic adhesion parameters and mechanical properties is then measured by: (1) altering the adhesion strength by increasing or decreasing ligand concentration at the bead surface, (2) altering CSK integrity by treating cells with cytochalasin D, (3) stimulating the stress-hardening response by increasing the exerted torque, (4) changing the cell environment from 2D to 3D while using low and high collagen concentrations. Results confirm that the proposed measure and analysis of the cell response to bead twisting can efficiently reveal some hidden molecular effects at the level of integrin–receptor adhesion while preserving cellular integrity. This last condition is required for measuring the cell mechanical response as well as the status of cellular adhesion in effective living cell conditions. From a theoretical point of view, stochastic models written for two opposed multiple bond configurations (namely zipper and parallel) are used, providing estimate of the bond number and how the molecular arrangement changes throughout the various experimental conditions studied.

2 Methods

2.1 The effect of magnetic bead twisting on cellular and molecular responses

By principle, in magnetic bead-twisting cytometry (MTC), functionalized ferromagnetic beads are deposited onto living cells. After adhesion on transmembrane receptors of the integrin type, the beads are partially embedded in the cytoplasm and become mechanically linked to the cytoskeleton. The use of MTC has largely contributed to demonstrate the leading role of integrin transmembrane receptors in the force-induced mechanochemical signaling and to establish the concept of mechanotransduction (Wang et al. 1993). More recently, a similar bead-twisting system has been used to reveal some of the deep components of mechanotransduction, e.g., the microtubules (Na et al. 2008); the Cajal bodies in the nucleus (Poh et al. 2012).

Applying a uniform magnetic field $\mathbf{H}$ generates a controlled magnetic torque $\mathbf{C}$ on the cytoskeleton and the interfacial molecular bonds (see Fig. 1) given by:

$$\mathbf{C} = \mu_0\, \mathbf{m} \times \mathbf{H}\,,$$
$$\text{i.e.,}\quad C = \mu_0 m H\ \sin\left(\frac{\pi}{2} - \theta_{\text{clamp}}\right) \tag{1}$$

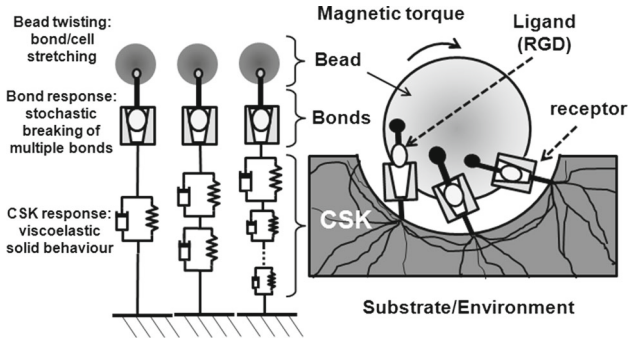

Fig. 1 Sketch of the bead-cell system (*right panel*) and equivalent molecular and cellular models (*left panel*) used to analyze the cellular response to the loading by magnetic bead. Receptors of the integrin type expressed at the apical face of epithelial cells bind the RGD ligands covering the beads. The integrin–RGD bonds are stretched during 1 min of application of an almost constant magnetic torque. The wide majority of these bonds survive to bead twisting and transmit the torque to the cytoskeleton whose rigidity control the bead rotation. Classical viscoelastic solid-like models with one or more elements (see the *left panel*) are used to determine the elastic modulus and the viscoelastic time constant proper to each component. The non-surviving bonds are supposed to break randomly during the minute of torque application. The kinetics parameters of this de-adhesion process can be described by a Bell-type model modified to take into account the multiplicity of the bead-cell molecular bonds

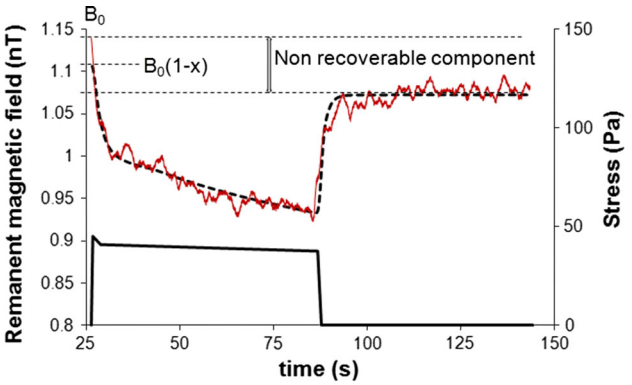

Fig. 2 Typical time-dependent MTC signals showing (1) the stress (in *Pascals*) exerted on the cell by the magnetic beads which includes an almost constant stress followed by a relaxation period (*bottom* signal, scale on the right side), (2) the measured remanent magnetic field signal ($1\ \text{nT}=10^{-9}$ Tesla) in the course of a given MTC experiment (*continuous line* on the *upper* signals, scale in the left side), (3) the fitting by the multiscale mechanical model (1 Voigt component of a viscoelastic solid-like model) obtained by a least squared method (*dotted line* on the *upper* signals). Note that, at the onset of stress application, the initial remanent field decreases suddenly from B_0 to $B_0(1-x)$ where x is the proportion of free rotating beads, i.e., the beads which fail to bond to the CSK and turn immediately by 90° right after torque application (see text for explanations). The *vertical arrow* indicate the non-recoverable component of the cell deformation signal used to determine the adhesion response. The complementary (recoverable) component of the signal is used to determine the viscoelastic properties of the CSK which are assumed to be constant over the minute of torque application, i.e., the cellular system remains pseudo stable over such a short time

where m is the modulus of the bead magnetic moment (the vector $\mathbf{m}$) which is obtained by calibration (e.g., $m \approx 2.3\ 10^{-13}$ A.m^2) and μ_0 is the permeability of the free space. θ_{clamp} is the bead rotation angle near equilibrium. In present experiments, we applied a transient step of loading (see the stress signal in Fig. 2) generated by a constant current intensity in Helmholtz coils and resulting in a clamp of 1 min. duration followed by a relaxation of 1 min. duration. The predetermined torque level in experiments below is basically 880 pN × μm, but this value can be modified in the range 400–1200 pN × μm (Féréol et al. 2008) by changing the current intensity. The magnetic torque translates into an apparent stress after dividing the torque by bead volume and applying a correcting factor κ for geometric effects (Ohayon et al. 2004; Féréol et al. 2006):

$$\sigma = \frac{\sigma_{\text{app}}}{\kappa} \tag{2}$$

This factor κ ranges from values below 0.1 at low bead immersion to values approaching 2 for complete bead immersion. $\kappa \approx 0.5$ corresponds to the half bead immersion characterizing the cell type presently studied. Under present culture conditions, the effective "mean" stress is in the range 40–80 Pa and varies only little during the minute of torque application (see Fig. 2). However, since MTC generates a torque, the stress distribution around the bead cannot be uniform. This has been clearly shown in several model studies in which a finite element model of the bead-cell mechanical interactions is developed (Ohayon et al. 2004; Mijailovich et al. 2002). It appears that the magnetic torque produces complex spatial stress/strain fields with shear dominating at the lower part of the bead while stretch and compression dominate on the diametrically opposed side located at the cell surface level, see Fig. 4 in Ohayon et al. (2004).

This load is exerted through transmembrane mechanoreceptors which act as physical bridges between the beads and the intracellular structure. These interfacial bonds are purposely used to transmit a 3D loading in the form of a magnetic torque as initially shown in Wang et al. (1993). In the present study, we focus on the decomposition of the deformation signal into a recoverable and non-recoverable components called $\theta_R(t)$ and $\theta_{NR}(t)$ (Fig. 3). The measured bead rotation angle $\theta_m(t)$ can be written:

$$\theta_m(t) = \theta_R(t) + \theta_{NR}(t) \tag{3}$$

The recoverable component of cell deformation $\theta_R(t)$ is attributed—as classically done—to the viscoelastic response of intracellular structure, e.g., a solid-like cell model whose number of characteristic time constants may be modified, depending on the number of CSK components that are taken into account. In the present study (see Fig. 1), we tested three such models with, respectively, one component as in Wang

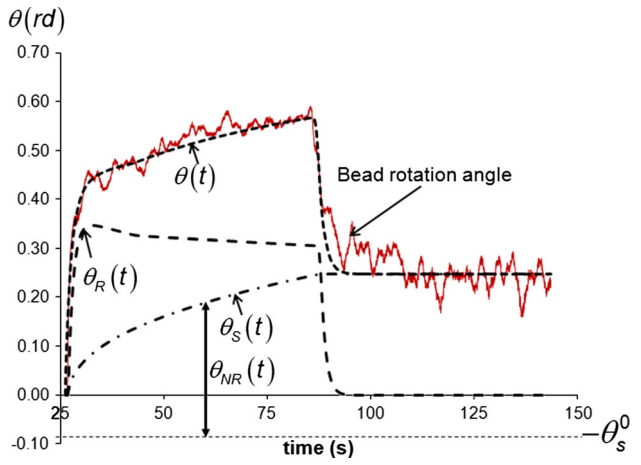

Fig. 3 The cell deformation experimentally measured (*continuous line* in *red*) is shown versus time in seconds. It is obtained after transformation of the relative change in remanent signal into bead rotation angle (in *radians*) by the arcosine function. The multiscale model used to fit the experimental data is shown by the thick dotted curve $\theta(t)$ which is at each instant the sum of two components: the reversible component $\theta_R(t)$, the non reversible component $\theta_{NR}(t)$. The time-dependent sliding component $\theta_S(t)$ and the immediate time-independent sliding component θ_S^0 corresponding to beads unbound to the cytoskeleton are also shown by semi interrupted curves

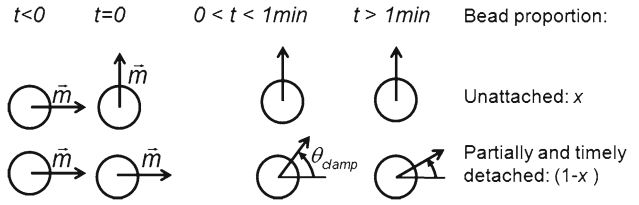

Fig. 4 Sketch defining the various bead angle components used to analyze the cellular and molecular responses. The model assumes a small proportion "x" of free rotating beads (unattached beads) which turn by 90° as soon as the magnetic torque is applied ($t = 0$). These beads instantaneously reach a 90° rotation angle which remains unchanged during torque and relaxation. These beads collectively contribute to the time-independent sliding component θ_S^0. The majority of the beads $(1 - x)$ contribute to the time-dependent cell response signal through a reversible $\theta_R(t)$ which is related to the viscoelastic response, and an irreversible component $\theta_{NR}(t)$ which is related to the probability of bond detachment. θ_{clamp} is the bead position reached near equilibrium after 1 min of torque application. The bead position during relaxation differs from the initial bead position because of partial bead detachment during the clamping period

et al. (1993); two components as in Laurent et al. (2003)) and n components for the power law model as shown by Balland (2006). We presently consider that the non-recoverable component of cell deformation, $\theta_{NR}(t)$, corresponds to molecular phenomena occurring primarily at the bead–cell interface. The probability of breaking molecular bonds at the cell–bead interface is indeed much higher than anywhere else in the cell, meaning that interfacial bonds are the weakest compared with intracellular bonds. We also assume that $\theta_{NR}(t)$ has a time-dependent and time-independent components which reflect molecular bonds having respectively effective and non effective linkages to the actin CSK. Namely:

$$\theta_{NR}(t) = \theta_s(t) + \theta_s^0 \tag{4}$$

$\theta_s(t)$ is a time-dependent sliding angle representing a variable amount of de-adhesion occurring during a given MTC loading. $\theta_s(t)$ is related to the probability of bond survival $P(t)$ through the simple arccosine function so that $P(t) = 1$ for $\theta_s(t) = 0$, and $P(t) = 0$ for $\theta_s(t) = \pi/2$:

$$\theta_s(t) = \arccos\left(P(t)\right) \tag{5}$$

θ_s^0 is a time-independent sliding component reflecting the few percent of adhesion sites that instantaneously dissociate at the onset of the loading, i.e., due to complete defect in CSK attachments (Fabry et al. 1999). Calling "x" the proportion of free rotating beads, the following expression is used to relate the difference: $\theta_m(t) - \theta_s^0$, to the decay, from B_0, in the projected magnetic field $B(t)$ during loading:

$$\theta_m(t) - \theta_s^0 = \arccos\left(\frac{B(t)}{B_0(1-x)}\right) \tag{6}$$

Free rotating beads actually quantify the number of immature adhesion sites whose connection with the CSK is too weak to resist loading. These immature bonds break instantaneously so free magnetic beads align in the direction of the perpendicular field **H** (Eq. (1)). Thereby, the parameter x represents the proportion of immature bonds in a given cell culture. Based on Eq. (6), the time-dependent MTC signal can be equivalently represented in terms of the decay of the remanent magnetic moment $B(t)$ or in terms of bead deviation angle $\theta(t)$ (as shown in Figs. 2 and 3 respectively).

2.2 Characterization of the complex bead–cell attachment

To characterize the molecular attachment between a given coated bead and the cell surface, we presently postulate that interfacial bonds between the bead and the cell will break in priority because they are the weakest molecular structures of the system. On the other hand, association of multiple bonds constitutes a general mechanism of molecular reinforcement which provide adequate levels of adhesion strengthening that single bonds could not sustain. Association of multiple bonds is also the pertinent assumption in most of culture conditions where contact area and surface chemistry between probe and cell are complex and not fully controlled (Williams 2003). The classical way to describe the global lifetime of a multiple molecular bond with a necessarily complex energy landscape is predicted by the Kramer–Smoluchowski theory (Evans 1998, 2001; Tsukasaki et al. 2007). This theory states that the global lifetime needed to transit across the n sharp ener-

getic barriers is the sum of the times needed to transit across individual barriers, namely:

$$T_{\text{off}}(t) = \sum_{n=1}^{N} \left(t_{\text{off}}^{0}(n) \exp\left(-\frac{f}{f_{\beta}(n)} \right) \right) \tag{7}$$

Equation (7) implies that multiple bonds with complex energy barriers make molecular interactions more durable, i.e., they survive longer when submitted to larger force, even though force still dramatically shorten each individual bond lifetimes (Evans 1998). Note that the bonds whose collective behavior is depicted by Eq. (7) are said to behave *non cooperatively* meaning that they are not supposed to break at the same time but stochastically, following their own kinetic response. They differ from the cooperative bonds which break simultaneously and thus behave as a unique equivalent bond with an energy barrier which is simply the sum of individual energy barrier height (Zhang and Moy 2003). In Eq. (7), each bond is independently affected by the force which is the signature of uncooperative bonds. $t_{\text{off}}^{0}(n)$ is the time for forward passage of the nth barrier:

$$t_{\text{off}}^{0}(n) = t_D \exp\left(\frac{E_b(n)}{k_B T} \right), \tag{8}$$

and where $E_b(n)$ is the barrier height of the potential chemical energy above the bound state, $k_B T$ is the thermal energy scale ($\approx$ 4 pN $\times$ nm), t_D is the Brownian time ($\approx 10^{-9} - 10^{-10}$s). $f_{\beta}(n)$ is the force scale of individual barriers:

$$f_{\beta}(n) = \frac{k_B T}{x_{\beta}(n)} \tag{9}$$

which is of the order of, e.g., 13 pN for integrins (Evans and Kinoshita 2007). $x_{\beta}(n)$ is in the range (0.1–1 nm) and represents the stretching distance at which the barrier is located (transitional state). For stretching larger than this distance, the bond becomes unstable. For a vanishing force in Eq. (7), one obtains the global natural lifetime which basically corresponds to the overall chemical energy level of the collective bond:

$$T_{\text{off}}^{0} = \sum_{i=1}^{N} t_{\text{off}}^{0}(n) = \frac{1}{K_{\text{off}}^{0}} \tag{10}$$

A major assumption of the present approach is to postulate that multiple bonds, although working uncooperatively, still behave as a "unique" or global bond obeying a Bell-type model, rewritten herein for a stress calculated from the attachment area at the bead–cell interface:

$$K_{\text{off}}(\sigma) = K_{\text{off}}^{0} \exp\left(\frac{\sigma}{\sigma_c} \right) \tag{11}$$

Accordingly, the stress-dependent dissociation rate $K_{\text{off}}(\sigma)$ is exponentially increased by the normalized stress. The parameters, K_{off}^{0} and σ_c, appear to be the two key parameters characterizing the kinetics of complex bond structures. The natural dissociation rate K_{off}^{0} is defined by Eq. (10) at zero force and the characteristic stress σ_c is related to bond characteristic forces (Eq. (9)). Note that it is not obvious that expressions of $K_{\text{off}}(\sigma)$ given by Eq. (11) and its reciprocal given by Eq. (7) are mathematically identical.

We have recently shown, by comparing simplified bond structures made of N-independent bonds with identical energy barriers working either in zipper mode or in parallel mode (see present "Appendix" and Isabey et al. (2013)) that the global behavior still obey a Bell-type model whose prefactors and exponent are affected by the bond number in a way depending on the bond configuration. For instance, the N-dependence of the normalized natural dissociation rates for the zipper and the parallel configurations are respectively:

$$\left[\frac{k_{\text{off}}^{0}}{K_{\text{off}}^{0}} \right]_{\text{zipper}} \approx N \tag{12}$$

$$\text{and} \quad \left[\frac{k_{\text{off}}^{0}}{K_{\text{off}}^{0}} \right]_{\text{parallel}} = \sum_{i=1}^{N \to +\infty} \frac{1}{n} \approx \ln(N), \tag{13}$$

and for the exponent, σ/σ_c, is such that:

$$\left[\frac{\sigma_c}{\sigma_{\beta}} \right]_{\text{zipper}} \approx 1, \qquad \left[\frac{\sigma_c}{\sigma_{\beta}} \right]_{\text{parallel}} \approx N, \tag{14}$$

where σ_{β} is the single bond stress related to the characteristic force f_{β} exerted at the bead–cell interface. On the whole, it can be said that specific models made of uncooperative bonds of identical energy predict a global behavior still obeying a Bell-type model with parameters depending on the bond configuration and variably on bond number N.

2.3 Relation between dissociation rate and probability of bond detachment

For single or multiple bonds working cooperatively (Evans 2001) or non cooperatively (Williams 2003), bond breakage, in the absence of rebinding, can be described by a first-order Markov process using a "single" time-dependent dissociation rate, $K_{\text{off}}(\sigma(t))$, which is related to the probability of bond survival, $P(t)$, by a simple first-order differential equation:

$$\frac{dP(t)}{P(t)} = K_{\text{off}}(\sigma(t))\, dt \tag{15}$$

or equivalently

$$P(t) = \exp\left[-\int_0^t K_{\text{off}}\left(\sigma(t')\right) dt'\right] \tag{16}$$

This Markovian approach applies to a multiple bond system to the extent that the integrated response resembles a "unique" bond. This has been clearly demonstrated for cooperative bonds breaking simultaneously at a barrier level which is the sum of individual barrier heights (Evans 2001). The application to uncooperative bonds is not so straightforward because bonds break randomly with their own force-dependent kinetic response (Eq. (7)). However, such approach is still applicable in the two simplified cases of loading: parallel and zipper, as shown in the Appendix. $P(t)$ represents the probability of survival for a collective bond.

Based on Eq. (16), analytical solutions for $K_{\text{off}}(\sigma(t))$ can be determined from the knowledge of $P(t)$ in the case of "force clamp" corresponding to a constant imposed stress ($\sigma(t) \approx \sigma$) (Fig. 2). Although this approach was initially proposed to probe single-molecule receptor–cytoskeletal anchoring (Evans and Kinoshita 2007), it can be extended to multiple bonds as long as the governing equation is similar to Eq. (16). The solution corresponding to a clamping process similar to the one used experimentally (Fig. 2) is given by:

$$P(t) = \exp\left[-K_{\text{off}}(\sigma) \times t\right] \tag{17}$$

meaning that $K_{\text{off}}(\sigma)$ can simply be obtained from the slope of the linear relationship between $(ln\,P(t))$ and t.

2.4 Obtaining cellular viscoelastic properties

The recoverable component of bead rotation was used to estimate the viscoelastic properties of the cell in response to the transient step loading as previously done (Féréol et al. 2008). The relationship between strain $\theta_R(t)$ and stress σ depends on the total history of the loading, up to the time t Fung (1981):

$$\theta_R(t) = c(t)\,\sigma_0 + \int_0^t c\left(t - t'\right) \frac{d\sigma}{dt}(t')\, dt' \tag{18}$$

where $c(t)$ is the creep function, i.e., the strain generated by a step stress, normalized by a constant stress value σ_0. The microrheological models proposed in the literature to describe the cell structure response are of similar nature, i.e., a viscoelastic solid with 1, 2, or "n" Voigt components.
$c(t) = \frac{1}{E} + \frac{t}{\eta}$ (single-Voigt model), i.e.,

$$\theta_R(t) \approx \frac{\sigma_0}{E}\left(1 - \exp\left(-\frac{t}{T}\right)\right) \tag{19}$$

$c(t) = \frac{1}{E_1} + \frac{t}{\eta_1} + \frac{1}{E_2} + \frac{t}{\eta_2}$ (double-Voigt model), i.e.,

$$\theta_R(t) \approx \frac{\sigma_0}{E_1}\left(1 - \exp\left(-\frac{t}{T_1}\right)\right) + \frac{\sigma_0}{E_2}\left(1 - \exp\left(-\frac{t}{T_2}\right)\right) \tag{20}$$

E, E_1, and E_2 are the elasticity moduli, (i.e., close to shear moduli since a magnetic torque is exerted) and η, η_1, and η_2 are the dissipation moduli (e.g., due to friction between CSK elements in a confined volume with steric properties) for the single-Voigt and the double-Voigt models respectively. Viscoelastic response time can be deduced from: $T = \frac{\eta}{E}$ or $T_1 = \frac{\eta}{E_1}$, $T_1 = \frac{\eta}{E_1}$ reflecting the viscoelastic responses of the overall CSK structure or its cortical and deep components ($T_1 < T_2$), respectively (Laurent et al. 2003). The time-invariant power law represents an alternative model more recently proposed (Fabry 2003; Trepat et al. 2004) which has been shown to correspond to an infinite series of viscoelastic solids (Balland 2006):

$$c(t) = A_0\left(\frac{t}{T_0}\right)^{\alpha}, \text{ i.e., } \theta_R(t) \approx \sigma_0\, A_0\left(\frac{t}{T_0}\right)^{\alpha} \tag{21}$$

The exponent α varies little, i.e., between 0 (solid-like) and 1 (fluid-like) and practically between 0.1–0.3 in living cells, a result consistent with the solid-like behavior assumption. The prefactor A_0 is inversely related to the modulus of elasticity, T_0 being an arbitrary response time fixed at 1 s. The cytoskeleton structure is modeled by infinite assembly units labeled by the index k, each of them showing a single Voigt model behavior with a viscoelastic response time T_k. Characteristic response times are thereby multiple and distributed according to an ideal power law: $T_k = T_m k^{\left(\frac{-1}{1-\alpha}\right)}$, where T_m is the largest relaxation time in the cell.

2.5 Experimental procedures

2.5.1 Cell cultures

A549 human alveolar epithelial cells (American Type Culture Collection, Rock-ville, MD, USA) were grown to confluence in DMEM containing 10 % FBS, 2 mM L-glutamine, 50 IU/ml penicillin, 50 µg/ml streptomycin, and incubated in a 5 % CO2 95 % air atmosphere. Routine subcultures (passages 89 to 92) were performed at 1/20 split ratios by incubation with 0.025 g/100 ml trypsin-0.02 g/100 ml EDTA in calcium- and magnesium-free DPBS for 10 min at 37 °C. For magnetic twisting cytometry experiments in 2D cell cultures, 96-well bacteriologic dishes were coated with fibronectin at a concentration of 5 $\mu g/cm^2$ for 3 h at 37 °C in incu-

bator. Cells were plated at the density of 70×10^3 per well in complete medium with serum, 48 h before experiments and incubated in serum-free medium with 1 % of BSA for 30 min before magnetic twisting cytometry experiments. For magnetic twisting cytometry experiments in 3D cell cultures, a 3D collagen matrix was used, providing a physiologically relevant cellular environment of adjustable stiffness (Jiang and Grinnell 2005). Interestingly enough, matrix stiffness and matrix pore size can easily been changed by changing the concentration of collagen; the higher the collagen concentration, the stiffer the gel and the smaller the pore size (Friedl and Brocker 2000). At the same time, MTC can advantageously be used in such a matrix because remanent bead magnetic field can easily be measured in a 3D reference volume instead of a 2D culture. Levels of remanent bead magnetic field in 3D matrixes are not different from the 2D and not different between stiff and soft gels (Tables 1–3 in Supplementary Material). A549 cells previously used in 2D substrates were cultured in 3D-environments of type I collagen. Two different concentrations of collagen were tested, i.e., 1 mg/ml to 5 mg/ml, enabling changing matrix stiffness; the higher the type I collagen concentration, the stiffer the gel.

2.5.2 MTC setup

The laboratory-made magnetic twisting cytometry device used in this study has been previously described (Laurent et al. 2003; Féréol et al. 2009). Carboxyl ferromagnetic beads (4.5 μm in diameter, Spherotec Inc., IL USA) were coated with arginine-glycine-aspartic acid (RGD) peptide according to the company's procedure (Telios Pharmaceuticals Inc., CA USA). Before use, coated beads were incubated in serum-free medium supplemented with 1 % BSA for at least 30 min at 37°C to block non-specific bindings. Ligand density can be changed by changing the concentration of RGD during bead coating. Starting with a standard RGD concentration value of 0.4 mg/ml during control conditions, six RGD concentrations have been tested corresponding to concentrations modified by a factor of 0.1, 0.2, 0.5, 2, 5 and 10. Beads were then added to the cells (40 μg of beads per well corresponding to a RGD density of about 1 RGD peptide/nm^2) for 20 min at 37C in a 5 % CO2 95 % air incubator. Unbound beads were washed away three times with serum-free medium 1 % BSA. Microbeads were then magnetized using a 0.15 T uniform short magnetic pulse (150 ms). This magnetic field is horizontal, i.e., parallel to the monolayer of adherent cells. The magnetic torque, C, (Eq. (1)) was then created by Helmholtz coils, which generate a vertical uniform magnetic field H ($H \leq 6.3$ mT) whose intensity is two orders of magnitude lower than magnetization field in order to avoid re-magnetization. Standard torque value used in present experiments is 880 pN × μm unless specified. This magnetic torque induces a bead rotation which is measured by a magnetometer that continuously measures the average projection of the bead remanent magnetic field $B(t)$ in the plane of the cell monolayer. The variations of $B(t)$, are measured with a magnetometer equipped with low noise probes, i.e., 0.14 nT, for a range of bead remanent magnetic field of the order of 1 nT (see Fig. 2).

2.5.3 Statistics

Assessment of cellular and molecular parameters were obtained by best fitting between model and MTC signal using a least square method based on Levenberg–Marquardt algorithm. Comparison of the mean value of mechanical and adhesion parameters between the different biological conditions tested was performed with statistical software package (Statistica v7.1, Stat Soft°$led\,R$, France) using non parametric test (Kruskal–Wallis test or Mann–Whitney U test). A p value smaller than 0.05 was considered significant.

3 Results

We present below the concurrent assessment of mechanical and adhesion properties by magnetic bead twisting based on a refined analysis of the non reversible component of bead rotation supported by the multiple bond theory summarized in Method and in "Appendix." To test the cellular and molecular sensitivity of this refined bead twisting method, we purposely explored the cellular and molecular response in modified intracellular or extracellular conditions such as: (1) weakening or reinforcing adhesion, (2) weakening or (3) strengthening CSK, (4) substituting a 3D environment for the classical 2D environment and modifying its stiffness. These various conditions are expected to modify the cellular and molecular properties in predictable directions and the proposed method aims at quantifying these modifications. In Figs. 5, 6, 7, and 8, adhesion parameters are systematically expressed in terms of the natural dissociation rate K^0_{off} and a characteristic stress σ_c, while mechanical properties are expressed in terms of CSK elastic modulus E and viscoelastic response time T based on the single-Voigt model (Table 1 in Supplementary Material). Results obtained with the two additional multicompartmental viscoelastic solid models are presented in Tables 1–3 in Supplementary Material for the mean values and SEM.

3.1 Effect of weakening/strengthening adhesion in a 2D culture

In the experiments shown in Fig. 5a–d, we modified bead coating density by changing RGD concentration from the basal state (0.4 mg/ml). RGD concentration was thus decreased by factors of 2 (0.2 mg/ml), 5 (0.08 mg/ml), and

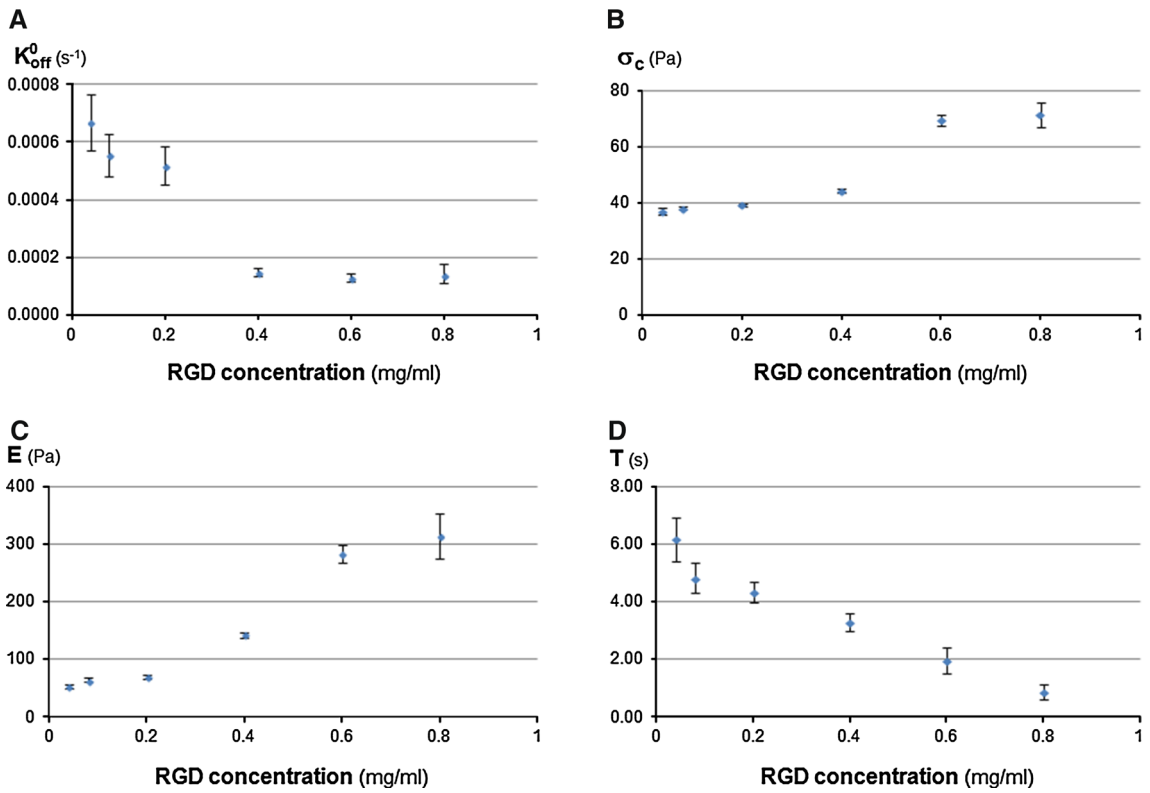

Fig. 5 Mean values and SEM of (i) adhesion parameters: natural dissociation rate K^0_{off} in s^{-1} (**a**) and reference stress σ_0 in Pa (**b**) and (ii) CSK mechanical properties: CSK elastic modulus E in Pa (**c**) and viscoelastic response time T in s (**d**) for the single-Voigt model, are obtained in cultured A549 cells for different RGD concentrations in the range 0.04–0.8 mg/ml. Standard RGD concentration value used in all other conditions is fixed at 0.4 mg/ml. For all parameters, large statistical differences ($p < 0.001$) are observed between low and high concentration. A RGD concentration of 0.4 mg/ml corresponds an initial remanent magnetic field of about 1 nT which is used as a basal value for the other experimental conditions presently studied. Except for the two lowest and the highest values of RGD concentration studied, differences within the values obtained for studied parameters are all highly significant ($p < 0.001$) for E and σ_0 and between slightly ($p < 0.05$) to highly ($p < 0.001$) significant for T and K^0_{off}

10 (0.04 mg/ml) or increased by factors of 1.5 (0.6 mg/ml), 2 (0.8 mg/ml) as shown in Fig. 5a–d. Beads acting as small matrixes bound to the cells through integrin–RGD binding constitute as much as probes to assess the state of cell–matrix adhesion at a given instant and for a given condition. Clearly, RGD concentration deeply modifies the molecular properties as shown by the significant differences between data obtained at low and high RGD concentration. The decay in natural dissociation rate is synonymous of bond stabilization which is permitted by the increase in ligand concentration. The increase in characteristic stress suggests some adhesion remodeling in response to the specific conditions studied. An important feature shown by Fig. 5a–d is that relationships existing between RGD concentration and the molecular (K^0_{off} and σ_c) or cellular (E and T) parameters are non linear. Such a nonlinear behavior has already been described in the literature as potentially related to the heterogeneity of RGD surface distribution at the nanometer scale and to the stochastic nature of the hydrolysis process (Lagunas et al. 2012). Consistently with the present results, the number of totally immature bonds seems to be significantly decreased (from 9 to 1 %) as ligand concentration increases (see Table 1 in Supplementary Material). Using different viscoelastic models does not modify these results. Indeed, in Table 2 and Table 3 (in Supplementary Material), the natural dissociation rates decrease nonsignificantly with the double-Voigt model and quite significantly with the power law model.

Mechanical properties of the cytoskeleton are modified in parallel to adhesion reinforcement, (i.e., E increases and T decreases). The stronger the adhesion, the higher the CSK recruitment, which is a result consistent with the literature (Burridge et al. 1988; Ingber 1997). Using viscoelastic solid models with more than one compartment does not deeply modifies the above results (See Tables 2 and 3 in Supplementary Material). The natural dissociation rates still decreases although nonsignificantly with the double-Voigt model but quite significantly with the power law model. In parallel, the rigidity modulus of the cortical and of the deep CSK com-

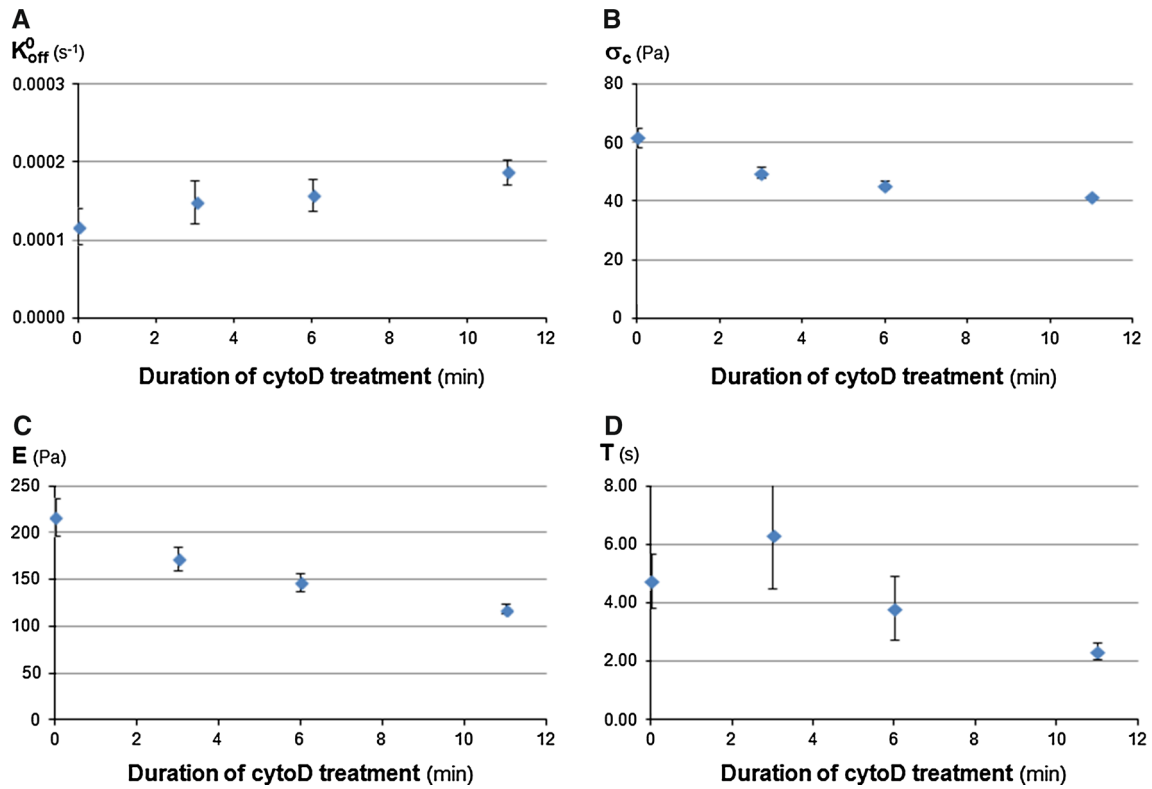

Fig. 6 Mean values and SEM of (i) adhesion parameters: natural dissociation rate K^0_{off} in s^{-1} (**a**) and reference stress σ_c in Pa (**b**) and (ii) CSK mechanical properties: CSK elastic modulus E in Pa (**c**) and viscoelastic response time T in s (**d**) for the single-Voigt model, are obtained in cultured A549 cells in the course of cytochalasin D treatment (time in minutes). The elastic modulus E exhibit a significant decay as time increases as well as σ_c. Only a slight increase in natural dissociation rate K^0_{off} is observed after 11 min of cytoD treatment. The viscoelastic response time T is never significantly changed compared to time zero. E is slightly ($p < 0.05$) decreased at 3 min. and highly decreased ($p < 0.001$) beyond. σ_c is highly decreased ($p < 0.001$) from 3 min. and above

ponents are both significantly increased as ligand density is increased, while the prefactor of the power law proportional to the inverse of the rigidity modulus is significantly decreased. In addition, the exponent of the power law is significantly decreased as ligand density is increased (Table 3 in Supplementary Material). This is the hallmark of a solidification process which confirms the pertinence of using solid-like models.

3.2 Effect of CSK weakening in a 2D culture

It has been constantly shown in tissue cells that depolymerizing actin filaments by cytochalasin D (cytoD treatment) results in CSK weakening and loss of internal tension (Wang et al. 1993; Wendling et al. 2000). Results presently obtained after 6 min are in agreement with previous results: The decrease in rigidity modulus is significant after cytoD treatment (Fig. 6c). Accordingly, the viscoelastic time constant T tends to decrease but less significantly. The diminution in CSK stiffness is the hallmark of a time-dependent alteration in actin structure induced by cytoD treatment. The effect of cytoD treatment on adhesion kinetics was not really measured before although it can be expected to remain small since cytoD is supposed to affect the intracellular CSK structure and not directly the transmembrane binding. Accordingly, the natural dissociation rate was only slightly increased (Fig. 6a). Likely for similar reasons, the quantity of totally immature adhesion bonds did not change and remained limited to 4 and 5 % (Table 1 in Supplementary Material). Surprisingly, the characteristic stress (Fig. 6b) appeared significantly decreased by cytoD treatment and by the time of treatment. The CSK alteration evidenced by the decay in rigidity modulus presently reported (Fig. 6c) and by the staining of actin structures before and after cytoD treatment already reported (Wendling et al. 2000) strongly suggests that direction of forces on the intracellular side could be modified as actin CSK is depolymerised. Moreover, if the decay in actin filaments number available for bond stretching was decreased by cytoD treatment, one may expect that force equilibrium and direction of tension between filaments will be changed, hence the observed significant decay in reference force reported in Fig. 6b. In summary, because cytoD

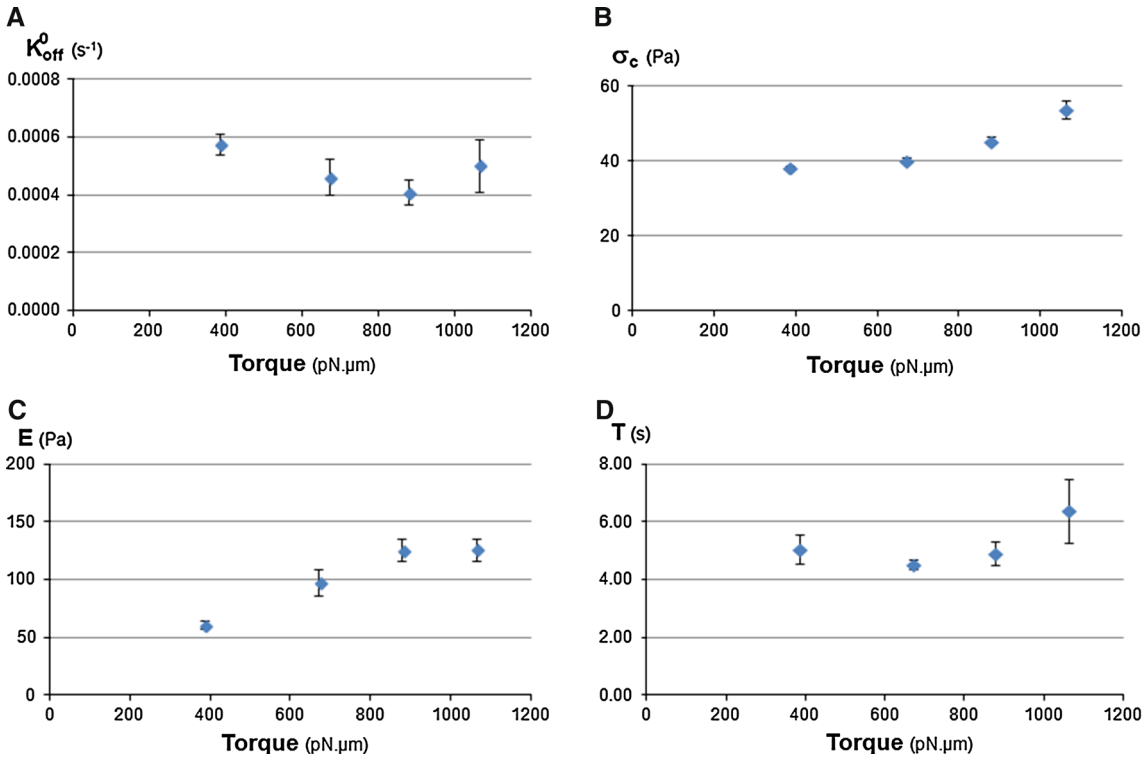

Fig. 7 Mean values and SEM of (i) adhesion parameters: natural dissociation rate K^0_{off} in s^{-1} (**a**) and reference stress σ_c in Pa (**b**) and (ii) CSK mechanical properties: CSK elastic modulus E in Pa (**c**) and viscoelastic response time T in s (**d**) for the single-Voigt model are obtained in cultured A549 cells for increasing torque in the range 380–1060 pN × µm. Standard torque value used in all other conditions is 880 pN.µm. The elastic modulus E exhibits a significant increase as torque increases as well as σ_c. The natural dissociation rate K^0_{off} and the viscoelastic response time T are not significantly affected for all torque levels tested. Significant differences in elastic modulus E are observed with the smallest torque. Values of reference stress σ_c are significantly changed between all torque conditions studied

treatment mainly targets the intracellular actin structure, it would minimally affect the chemical energy of interfacial bonds, hence the quasi constancy of K^0_{off} on the one hand (Fig. 6a). On the other hand, direction and magnitude of stress exerted on adhesion sites have some reason to be changed secondary to the CSK alteration leading to a sensitivity of the characteristic force to the bond number, namely a decrease in σ_c as duration of cytoD treatment remodels the force equilibrium throughout the cytoskeleton structure (Fig. 6b). Results obtained with the two other viscoelastic solid models globally confirm the results obtained with the single-component viscoelastic model, i.e., insignificant changes in the natural dissociation rate and significant time-dependent decay of the cortical and the deep rigidity modulus (Table 2 in Supplementary Material). Accordingly, the prefactor of the power law increases with the time of cytoD treatment (Table 3 in Supplementary Material). Yet, the exponent of the power law does not significantly change confirming that cytoD treatment mainly affects the intracellular internal tension (Wendling et al. 2000) while not necessarily affecting the nature (i.e., solid versus fluid) of the cellular material.

3.3 Effect of CSK strengthening in a 2D culture

Stress/strain hardening is a largely recognized behavior observed when mechanical loading is increased in adherent tissue cells such as epithelial cells (Féréol et al. 2008; Laurent et al. 2003; Potard et al. 1997) or endothelial cells, as revealed by the pioneering MTC experiments of Wang et al. (1993). Various mechanobiological models have been proposed: 3D deformation of the tensegral CSK structure (Wendling et al. 2000), hyperelasticity of the cellular material (Ohayon et al. 2004), and molecular motor activation induced by stress (Mizuno et al. 2007). The large cellular displacements induced by bead twisting (Féréol et al. 2009) are consistent with the observed stress-/strain-hardening behavior. Present data obtained in A549 epithelial cell lines tested at increasing torque levels confirm these earlier reported results, namely rigidity modulus significantly increases as stress increases for the three viscoelastic models tested (See Fig. 7c and Tables 1 and 3 in Supplementary Material). Note that this stress-/strain-hardening behavior remains the proper of highly structured tissue cells (Féréol et al. 2009) which may include stress redistribution throughout the CSK struc-

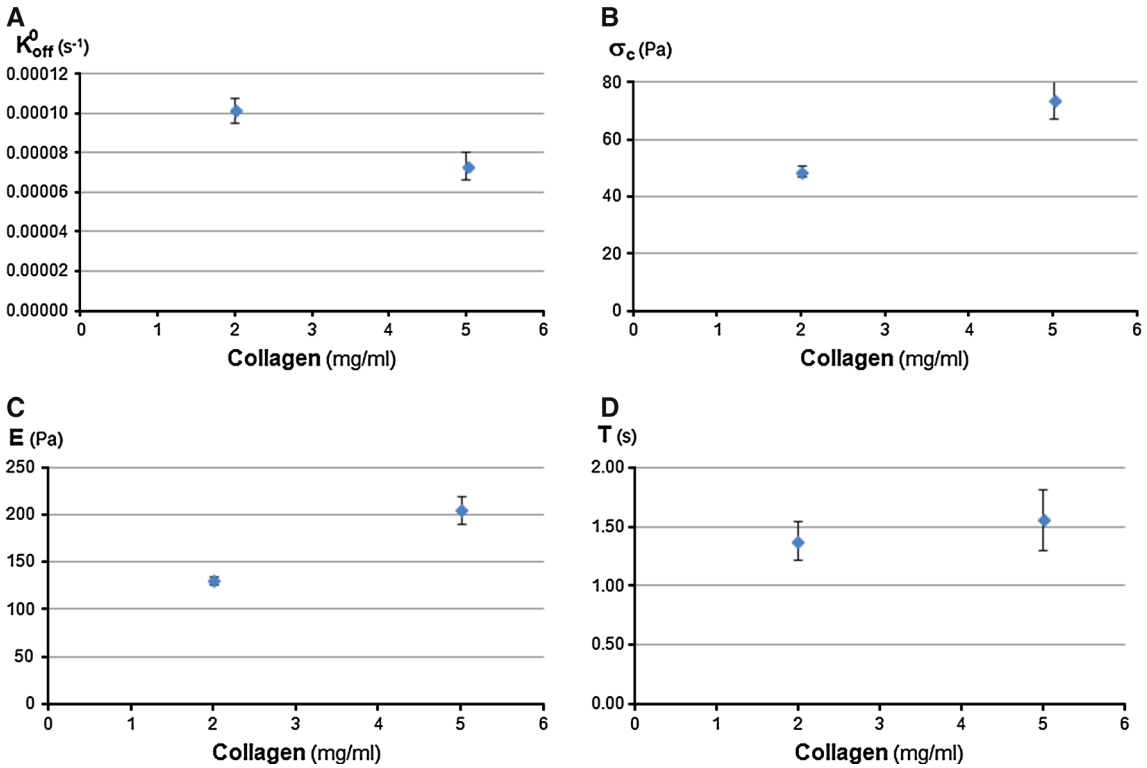

Fig. 8 Mean values and SEM of (i) adhesion parameters: natural dissociation rate K^0_{off} in s^{-1} (**a**) and reference stress σ_c in Pa (**b**) and (ii) CSK mechanical properties: CSK elastic modulus E in Pa (**c**) and viscoelastic response time T in s (**d**) for the single Voigt model, are obtained in A549 cells cultured in 3D matrix of type I collagen for low and high concentrations of collagen: 2 and 5 mg/ml. The elastic modulus E and the reference stress σ_c exhibit a significant increase in stiffer gel ($p < 0.01$ and $p < 0.001$ respectively), while the natural dissociation rate K^0_{off} is significantly decreased ($p < 0.01$). Viscoelastic response time T is not significantly affected

ture (Zhu et al. 2000) and the stimulation of integrin receptors loaded by magnetic beads (Pommerenke et al. 1996). Note also that the bead deviation angle remained almost constant in these experiments suggesting that stress hardening was revealed at almost constant deformation (see Tables 1–3 in Supplementary Material). The concomitant increase in loss modulus (data not presented) let the viscoelastic response time almost unchanged (Fig. 7d).

The unknown aspects enlightened by the present results concern the outcome of adhesion kinetics in the context of stress–strain hardening. We observed a nonsignificant decay in the natural dissociation rate K^0_{off} with the single-Voigt model (Fig. 7a) which is consistent with the idea that the stress-/strain-induced cellular remodeling is primarily intracellular and to a lesser extent interfacial. Yet, this decay becomes significant with the double-Voigt model (Table 2 in Supplementary Material). Moreover, as the torque level increases, there is a significant increase in the characteristic stress σ_c for the three models tested (Fig. 7b and Tables 1–3 in Supplementary Material) suggesting that redistribution of force across the bonds is more important than chemical reinforcement of receptor–ligand linkages. Such an evolution is consistent with a change in the interfacial force distribution in response to loading increase. In summary, CSK reinforcement (shown by Fig. 7c) results in an increase in the characteristic stress σ_c of adhesion, while weakening of CSK or adhesion (shown by Fig. 5 and 6) results in a decrease in the characteristic stress of adhesion sites suggesting that alterations in the distribution of stress at the level of interfacial bonds is an efficient mechanism of adhesion regulation by force.

3.4 Effect of 3D environments of various stiffness

Cellular response presently tested for the first time in 3D environments show that adhesion and mechanical properties are significantly modified by environmental stiffness. The direction of these evolutions is toward higher CSK stiffness (Fig. 8c) and stabilization of adhesion (Fig. 8a) in stiffer gels. This is consistent with the previously described adaptability of cells to their mechanical environment, i.e., cells in stiffer environments get stiffer and reinforce their anchorage (Féréol et al. 2009). Interestingly, such an increase in CSK stiffness is observed with the three viscoelastic models tested (Fig. 8c and Tables 1–3 in Supplementary Material). The stabilization of adhesion, attested by a signif-

icant decay in the natural dissociation rate is observed with the single (Fig. 8a) and the double-Voigt models (Table 2 in Supplementary Material). Incidentally, because viscous modulus is also significantly increased for the double-Voigt model, the viscoelastic response times show a nonsignificant decay (Fig. 8d). The characteristic stress σ_c is significantly increased for the stiffer gel whatever the viscoelastic model used (Fig. 8b and Tables 2–3 in Supplementary Material) suggesting that stiffer environment would result in stress redistribution and higher sensitivity of the characteristic stress σ_c to the bond number (see Appendix). The number of fully immature bonds is consistently decreased in stiffer gels for the three viscoelastic models tested (Tables 1–3 in Supplementary Material). On the whole, the results obtained by this new method are consistent with the concept of adaptability and sensitivity of both the cytoskeleton and the adhesion system to the mechanical properties of the cellular environment.

4 Discussion

4.1 Specific features of the proposed bead-twisting method

Altogether, present results confirm the validity of an extended Bell-type model to describe the multiple bond behavior at the bead-cell interface during magnetic bead twisting. Magnetic bead twisting appears a minimally destructive method enabling to obtain biologically and theoretically consistent parameters reflecting the evolution of cell adhesion state and CSK mechanical properties for a variety of cell alteration conditions. This is possible because the mechanical stresses generated by bead twisting remain in a physiological range and practically in a range of stress below 50 Pa. Moreover, the derivation of adhesion parameters from probabilistic equations is made for the dissociation rate and not for the rupture force, enabling to characterize adhesion with a minimal amount of bond breakage.

A basic assumption of the present method is to consider that the probability of breaking molecular bonds at the cell-bead interface is much higher than anywhere else in the cell. It means that although potentially activated secondary to conformational change of proteins, interfacial bonds are the weakest compared to intracellular molecular bonds. The weakness of interfacial bonds as well as their representativeness of adhesion state throughout the cell, are indeed standard assumptions in most of cell adhesion studies whenever one or several bonds are stretched and whatever the stretching method used, i.e., cell–cell or cell–probe (Evans and Kinoshita 2007; Pierres et al. 1996). A similar assumption may be applied for cells in 3D environments. Indeed, cell 3D matrix interactions are point like or string like; hence, they are spatially more restricted than a ligand-coated surface (Friedl and Brocker 2000). This suggests that attachment and detachment forces present at each individual interaction point are lower than upon interaction with planar ligand. Consistently, values of dissociation rate presently found in 3D are systematically smaller than those found in 2D.

To test the validity of these assumptions and beyond the capability of the proposed system to characterize adhesion and mechanical properties in living cells, we used the well known A549 cell line model (Féréol et al. 2008; Vlahakis et al. 1999). The mechanical behavior of these moderately contractile cells can be satisfactorily described by passive rheological models. The evolution of kinetic adhesion parameters and mechanical properties were both measured in these cells while successively altering intracellular, interfacial, or environmental conditions. We presently demonstrate that the proposed approach enables quantifying the effects of these alterations on both cellular adhesion and cytoskeleton mechanical response, while the overall evolution is in qualitative agreement with expected biological evolution. Indeed, adhesion stabilization and CSK stiffness can both be altered when one of the following conditions are changed: (i) RGD ligand concentration, (ii) mechanical loading, (iii) 3D environmental stiffness. By contrast, CSK stiffness and to a lesser extent bond stabilization are both decreased in the course of depolymerizing treatment by cytoD. In addition, lower attachment and detachment forces were consistently found for cells in 3D versus 2D environments as values of the natural dissociation rates were systematically lower in 3D compared to 2D substrates, i.e., $K_{\text{off}}^0 \leq 10^{-4}\ \text{s}^{-1}$ versus $K_{\text{off}}^0 > 10^{-4}\ \text{s}^{-1}$ respectively.

Noteworthy, the natural dissociation rate measured by this new method in planar cultured cells is roughly two orders of magnitude smaller than the natural dissociation rate reported in the literature for single-molecule interactions of integrin–ligand bonds, e.g., $k_{\text{off}}^0 = 0.015\ \text{s}^{-1}$ for fibronectin–integrin linkages tested on a purely bio-mimetic cell-free system (Kokkoli et al. 2004), or $k_{\text{off}}^0 = 0.012\ \text{s}^{-1}$ for single-molecule AFM measurements between K562 cells that express the $\alpha_5\beta_1$ integrins (Li et al. 2003). These values are both in agreement with the dissociation rate constant $k_{\text{off}}^0 = 0.01 s^{-1}$ reported between fibronectin and the $\alpha_5\beta_1$ fibronectin receptor on fibroblast cells in solution (Lauffenburger and Linderman 1993). The drastically reduced values of K_{off}^0 observed when measured by MTC can only be the result of multiple bond association but specifically through integrin attachment. In addition, the change in the reference stress σ_c values provide molecular information about the change in bond configuration and/or the change in bond number between the different studied conditions as explained below. It appears that these differences have led to deep modifications of these parameters. For instance, changing the density of collagen from 1 mg/ml to 5 mg/ml means huge

decrease in matrix pore size. Such a decrease in pore size leads to an increase in availability of matrix ligands which is presently detected by the method through the decay in K^0_{off} (Fig. 8a) and the increase in σ_c (Fig. 8b).

4.2 The multiple bond theory foundation

The present approach assumes that complex energy barriers can still be described by a Bell-type model (see Eq. (11)). The biological relevance of measured adhesion parameters K^0_{off} and σ_c, obtained with the multiple bond model in a bead twisting system where a number bonds is implicated supports this idea. The Bell model has been shown to be theoretically founded (Evans 2001; Bell 1978) and useful to analyze the kinetics of complex bond dissociation with force (Marshall et al. 2003). The pertinence of the Bell-type model has been demonstrated for single bonds probed by constant-force experiments such as atomic force microscopy (AFM) (Noy and Friddle 2013), optical tweezers (OT) (Choquet et al. 1997), biomembrane force probes (BFP) (Marshall et al. 2003), and multiple bonds using parallel plate flow chambers (PPFC) (Zhu et al. 2008). Real biological situations are usually much more complex in terms energy landscapes because a large number of biomolecules may interact at numerous sites (Evans 1998) while bond environments may be soft such as with flexible polymers (Evans and Ritchie 1999) and/or with highly deformable probes (Noy and Friddle 2013). Noteworthy, their kinetic behavior can still be described by a Bell-type model but with a prefactor modulated by a force-dependent function leading to: $K_{\text{off}}\left(\tilde{f}\right) = K^0_{\text{off}}\, g\left(\tilde{f}\right) \exp\left(\tilde{f}\right)$ where $g\left(\tilde{f}\right)$ means that force modifies the shape of the transition state barrier such that adding complexity to an energy landscape make the bond more durable at higher forces (Evans 1998). In the parallel model (see "Appendix" and Isabey et al. (2013)), we find: $g\left(\tilde{f}\right) \sim \left(\frac{\tilde{f}}{N}\right)^{0.5}$ ($\tilde{f} \neq 0$ and $N \geq 2$), which means that force (here normalized) tends to increase the prefactor dissociation rate while increasing N has the opposite effect. On the other hand, the exponent $f/(Nf_\beta)$ is supposed to increase with force and to decrease as N increases which means that force still lowers the barrier magnitude while N does the opposite thus stabilizing the bond.

The two idealistic models presented in Appendix represent two extreme cases of force distribution among the multiple bond structures. Indeed, the parallel configuration represents a fully homogeneous force distribution of a force directed perpendicularly to the bond plane, while the zipper configuration represents a fully heterogeneous force distribution with a force directed obliquely or tangentially to the bond plane and totally exerted on the leading bond (Isabey et al. 2013). These two bond configuration are obviously too idealistic compared to the biological complexity notably, because the stress or strain fields resulting from twisting of partially immersed beads are definitely multidirectional (3D) (Ohayon et al. 2004; Mijailovich et al. 2002). These two extreme configurations yet provide a wide range of possible bond structure, enabling to understand the evolution of adhesion parameters, i.e., K^0_{off} and σ_c. If we compare values for single bonds, i.e., $k^0_{\text{off}} \sim 0.01$ (Kokkoli et al. 2004; Li et al. 2003; Laufenburger and Linderman 1993), with experimental values presently obtained K^0_{off}: 1.10^{-4} s^{-1} – 5.10^{-4} s^{-1} (Tables 1–3 in Supplementary Material), we find values of $k^0_{\text{off}}/K^0_{\text{off}}$ in the range: 20–100. The number of receptor–ligand bonds can be deduced from the theoretical relationships between $k^0_{\text{off}}/K^0_{\text{off}}$ and N as shown in Isabey et al. (2013) which reveals the strong dependence on bond configuration of the ratio between single and multiple dissociation rates. With the zipper configuration, we have $k^0_{\text{off}}/K^0_{\text{off}} = N$, meaning that the range of $k^0_{\text{off}}/K^0_{\text{off}}$ is the range of N. However, in the zipper model, the bond number should not affect σ_c (see "Appendix"). This prediction is not verified experimentally, since significant variations of σ_c are found in most of studied conditions,(e.g., Fig. 5b), suggesting that the zipper configuration is not necessarily the most appropriate. By contrast, the parallel model predicts: $\sigma_c = N\sigma_\beta$. Typical values of σ_β can be estimated from single bond studies: $\sigma_\beta = f_\beta/A = 0.75$ Pa ($= 15$ pN/20 μm^2) Evans and Kinoshita (2007), while experimental values of reference stress are in the range : $\sigma_c = 35$–75 Pa (Table 1 in Supplementary Material). Thus, assuming the parallel model leads to bond number values in a similar range of values: $N \approx 50$–100.

Importantly, the significant changes in reference stress σ_c experimentally found in most of the studied conditions tested can be enlightened by the predictions of the multiple bond theory. More specifically, parallel configuration means N-dependence of the reference stress σ_c while zipper configuration does not. Thus a change in reference stress σ_c can be seen as a criteria pertinent of a change in bond configuration. An interesting result is that σ_c is a parameter susceptible to reveal a change in molecular bond configuration, e.g., from zipper to parallel or the reverse. The evolution of this parameter can also reflect if bond number increases or decreases. Interestingly enough, the parallel configurations seems widely appropriate to the experimental conditions studied since (i) increasing coating density results in an increase in σ_c consistent with the expected increase in N, (ii) depolymerising actin CSK results in a rapid decrease in σ_c consistent with a CSK remodeling affecting bond structure and reducing bond number, (iii) stress hardening as well as stiffer 3D environment both results in an increase in σ_c consistent with the redistribution of local forces exerted on bonds whose association might be increased. More specifically, compared to 2D, cells in 3D environments receive external forces and transmit the generated traction forces through all

the cell surfaces in contact with the surrounding extracellular matrix. This is susceptible to modify cell–matrix interactions and to modulate integrin receptors (Cukierman et al. 1998) meaning that local forces might redistribute in direction and magnitude which is reflected by the significant change in σ_c(shown in Fig. 8b).

4.3 The bead–cell binding

The monomeric RGD (arg-gly-asp) peptide motif derived from the cell-binding domain of fibronectin has been shown to interact with $\alpha_v\beta_3$ and $\alpha_5\beta_1$ integrins (Ruoslahti 1996). These transmembrane receptors mediate cell adhesion by forming links between extracellular matrix and cytoskeleton (Matthews et al. 2006). On the basal cell face, these links are used in cell motility because the actin cytoskeleton generate forces pulling the integrin and attached matrix molecules toward the cell center. The same rearward translocation movement can be demonstrated on apical cell face by attaching beads to integrins enabling to follow the pathway, the velocity, and forces developed by the cytoskeleton (Choquet et al. 1997). It has been shown that integrin clustering is essential for cytoskeletal attachment.

This is identically true for magnetic bead twisting where bead binding is used to transmit both the magnetic torque and the cell reaction force. Prior to loading, a sufficient time ($\sim$ 30 min) was let for bead incubation and attachment to the cell to permit ligand binding and integrin clustering. It has been shown that in presence of force and for bonds which resist force, 10 s is sufficient to increase the bond strength by recruiting additional cytoskeleton consistently with the findings of an immediate formation of actin cytoskeleton beneath the point of bead binding (Miyamoto et al. 1995). Typical integrin expression in highly adherent cells such as fibroblasts is of the order of 100,000 receptors per cell for a cell area of 1500 μm^2, yielding to a receptor density of approximately 50–100 integrins/μm^2 (Akiyama and Yamada 1985). Such a binding system enables to reach maximal values of force density of the order of 2 nN/μm^2 in cancer cells and 4 nN/μm^2 in fibroblasts (Stricker et al. 2011). It means that each integrin on the basal face can support a stress up to 80 pN/μm^2 ($\sim$Pa). By contrast, the apical density of integrins is highly dependent on cell type and polarization state. For instance, in epithelial cell lines such as A549, integrins are systematically expressed at apical face but in primary type II epithelial cells, integrins are not sufficiently expressed on apical cell face, rendering the direct probing of these cells by RGD-coated beads unlikely (Féréol et al. 2006, 2009). This suggests that the number of integrins per bead is most likely minimal in case of apical location. For a mean applied stress which does not exceed 50 pN/μm^2 (see Table 1 in Supplementary Material) and an estimated number of integrin–ligand bonds in the minimal range $N = 50 - 100$ for the 20 μm^2 of bead surface, we find an integrin density of 2.5–5 integrin/μm^2 which is much less than the integrin density found on cell basal face (see above). This apical integrin density corresponds to a maximal stress exerted of 10–20 pN ($\sim$Pa) per integrin which is the range of characteristics force found for isolated integrins f_β (Evans and Kinoshita 2007). Although integrin number is small, they may associate. Interestingly three integrins have been found to be necessary and sufficient to form clusters ensuring coupling to and translocation with actin cytoskeleton (Coussen et al. 2002). Therefore, the binding density on beads appears quite sufficient for an effective connection of the bead with the CSK. This estimate brings a new confirmation that the stress applied by the MTC technique is far from the maximal strength values that cell–substrate adhesion can support, i.e., $\sim$200 nN (Gallant et al. 2005).

4.4 Comparison with other micromanipulation techniques

In this study, we used the classical bead magnetic twisting cytometry device to successfully assess molecular and cellular properties not only in 2D but also in 3D environments. There are very few techniques permitting CSK-specific measurements of mechanical and adhesive properties both in 2D and in 3D. Using microfabricated arrays of elastomeric microneedle-like posts is an efficient way to manipulate and measure in planar cell culture conditions, the mechanical interaction of cells, knowing that the general morphology of cells on micropillars remains similar to that of cells cultured on planar substrates (Tan et al. 2003). In a similar fashion, we demonstrate that the magnetic twisting cytometry technique is able to reveal some hidden information on the cell–matrix interactions while not altering cellular integrity. This is because the beads act as non destructive sensors, i.e., similarly to the micropillar above, generating a minimal stress that leave the cell in a state which is as close as possible from normal culture conditions. In other words, bead probing of cell–matrix interactions is naturally performed through multiple bond stretching while bond stretching occurs directly at the cell surface with no room for tether formation nor for extensive bond breakage as required by the measure of rupture forces during AFM experiments (Noy and Friddle 2013). At the same time, the bead–cell displacement which occurs at the micrometer scale during bead twisting is huge compared to the bond size, a stretching condition which enables us to neglect the bond rebinding ($K_{on} \sim 0\ s^{-1}$). This is a new confirmation that the proposed method essentially aims at comparing cellular/molecular remodeling in between different experimental conditions.

There are indeed a number of criteria to follow if one wants to extract meaningful adhesion parameters from bond

studies. The most striking one are that stretching forces have to be placed into the mechanical, structural, and dynamical contexts proper the bond studied. Clearly, the bead-twisting system used herein enables us to stretch adhesion bonds while not altering cell integrity. Moreover, the fact that each bond is allowed to break randomly provides realistic conditions for measurement of mechanical and adhesion properties because of minimal destruction of intracellular and interfacial molecular bonds. If the loading rate regimes could not be deeply modified by the bead twisting technique, the large populations of beads ($\sim 10^5$) and bonds ($\sim 10^7$) involved in each experiment provide a statistical estimate of the multiple random molecular interactions occurring between CSK and cross-linking proteins on the one hand, and at the bead–cell interface on the other hand.

Thus the present approach can be seen as providing an homogenized response of both adhesion parameters and mechanical properties treated simultaneously and specifically (Ohayon et al. 2004). Indeed, the multiscale intracellular properties of the cytoskeleton are integrated into a few *integrated* viscoelastic parameters herein considered by three exchangeable solid-like models which provide complementary information which are obtained at different scales (Balland 2006). The shape of the loading signal, i.e., its frequency content, is unmodified in the course of present experiments, letting the three viscoelastic models tested provide more or less equivalent information about the deep nature of intracellular structure. Note that the power law model which includes a wide number of characteristic times for the structure, might take into account part of the molecular response and thus bring to a certain extent some redundancy. This might be the reason explaining why the evolution of adhesion parameters obtained with the models with more than two elements (Tables 2 and 3 in Supplementary Material) appears indeed less significant than the evolutions obtained with the one element solid-like model.

By combining experimental and theoretical approaches, we are able to achieve a multiscale assessment of (1) the CSK-specific cell adhesion system and (2) the CSK-specific internal structure. The same probing system, i.e., a CSK-specific probing system, is used to concomitantly (1) stretch CSK-specific cell surface bond receptors and (2) deform cell structure. Thus, this multiscale MTC enables extracting adhesion kinetics parameters and cell mechanical properties can be done at the same time and through the same maneuver, i.e., basically a clamp. We purposely used stochastic theory of multiple bond association and simplified bond configurations (e.g., zipper and parallel), to demonstrate that lifetime response of collective bonds breaking randomly can be described by a Bell-type model whose factors (natural dissociation rate and exponent) are modulated by bond number (Isabey et al. 2013). Advantageously, an equivalent "single bond" model can be used to describe the molecular and cellular responses to bead clamping maneuver and evaluated this response throughout a variety of biological conditions. Note that the bead twisting system used herein has already proven its high CSK specificity and capability to reveal hidden aspects of the CSK-mediated cell response (Na et al. 2008); the Cajal bodies in the nucleus (Poh et al. 2012). In summary, we presently demonstrate that cellular and molecular properties (here of A549 cell lines) can be simultaneously extracted from the response to loading by magnetic bead twisting of living cells either adherent to a planar 2D substrate or embedded in a 3D matrix of Type I collagen.

Acknowledgments The authors wish to thank Pr. J.B. Grotberg for long and fruitful discussions.

Appendix

To simplify the general solution given by Eq. (7), we consider N identical independent bonds working collectively and organized in two extreme cases of loading distribution, i.e., parallel where each attachment shares the same force, and zipper where all the force is experienced by a single leading edge attachment until failure when it is passed on the next.

For parallel:

$$T_{\mathrm{off}}(f) = t_{\mathrm{off}}^0 \sum_{n=1}^{N} \left(\frac{1}{n} \exp\left(-\frac{f}{n f_\beta} \right) \right) \approx \left[t_{\mathrm{off}}^0 \left(\frac{2f}{N f_\beta} \right)^{-0.5} \exp\left(-\frac{f}{N f_\beta} \right) \right]_{N \geq 2,\, f \neq 0} \tag{22}$$

For zipper:

$$T_{\mathrm{off}}(f) = t_{\mathrm{off}}^0 \sum_{n=1}^{N} \left(\exp\left(-\frac{f}{f_\beta} \right) \right) = t_{\mathrm{off}}^0 \; N \; \exp\left(-\frac{f}{f_\beta} \right) \tag{23}$$

The series appearing in Eqs. (22) and (23) have previously been proposed by Evans (2001) and Williams (2003). The analytical form in Eq. (23) has been initially given by Williams (2003) while that of Eq. (22) has been recently proposed by Isabey et al. (2013). Noteworthy, these analytical expressions describe overall lifetimes (conversely, the overall dissociation rate) suggesting that, to describe multiple bonds, a Bell-type model holds in very different conditions of loading $K_{\mathrm{off}}(f) = K_{\mathrm{off}}^0 \exp\left(\frac{f}{f_c} \right)$ similar to Eq. (11).

For parallel bonds, the prefactor of the Bell-type model is given by:

$$K_{\text{off}}^0 = k_{\text{off}}^0 \left[\sum_{n=1}^{N} \frac{1}{n}\right]^{-1} \approx \left[\frac{k_{\text{off}}^0}{0.6 + \ln N}\right]_{f=0, N\geq 10}$$

$$\text{or} \quad K_{\text{off}}^0 \approx k_{\text{off}}^0 \left(\frac{2f}{Nf_\beta}\right)^{0.5}_{f\neq 0, N\geq 2}$$

$$\text{and} \quad f_c = Nf_\beta \tag{24}$$

For zipper bonds:

$$K_{\text{off}}^0 = \left[\frac{k_{\text{off}}^0}{N}\right]_{f=0} \quad \text{and} \quad f_c = f_\beta \tag{25}$$

Application of a force to such a complex bond system made of several uncooperative identical weak bonds exponentiates its dissociation. This behavior resembles the single bond behavior predicted by the Bell-type model (Evans 2001; Evans and Kinoshita 2007; Evans and Ritchie 1997). However, at given force, bond association dramatically decreases the rate of dissociation compared to the single bond. In parallel bonds with homogeneous force redistribution at each step, the global dissociation rate is exponentially decreased as the bond number increases (Eq. (24)). In zipper bonds, the natural dissociation rate decreases linearly as number of bonds N increase independently on force level (Eq. (25)), while exponent is unaffected by N.

References

Akiyama SK, Yamada KM (1985) The interaction of plasma fibronectin with fibroblastic cells in suspension. J Biol Chem 260:4492–4500

Balland M et al (2006) Power laws in microrheology experiments on living cells: comparative analysis and modeling. Phys Rev E Stat Nonlin Soft Matter Phys 74:021911

Bell GI (1978) Models for the specific adhesion of cells to cells. Science 200:618–627

Burridge K, Fath K, Kelly T, Nuckolls G, Turner C (1988) Focal adhesions: transmembrane junctions between the extracellular matrix and the cytoskeleton. Annual review of cell biology 4:487–525. doi:10.1146/annurev.cb.04.110188.002415

Choquet D, Felsenfeld DP, Sheetz MP (1997) Extracellular matrix rigidity causes strengthening of integrin-cytoskeleton linkages. Cell 88:39–48

Coussen F, Choquet D, Sheetz MP, Erickson HP (2002) Trimers of the fibronectin cell adhesion domain localize to actin filament bundles and undergo rearward translocation. J Cell Sci 115:2581–2590

Cukierman E, Pankov R, Yamada KM (1998) Cell interactions with three-dimensional matrices. Curr Opin Cell Biol 14:633–639

Evans E (1998) Energy landscapes of biomolecular adhesion and receptor anchoring at interfaces explored with dynamic force spectroscopy. Faraday Discuss:1-16

Evans E (2001) Probing the relation between force-lifetime-and chemistry in single molecular bonds. Annu Rev Biophys Biomol Struct 30:105–128

Evans E, Kinoshita K (2007) Using force to probe single-molecule receptor-cytoskeletal anchoring beneath the surface of a living cell. Methods Cell Biol 83:373–396

Evans E, Ritchie K (1997) Dynamic strength of molecular adhesion bonds. Biophys J 72:1541–1555

Evans E, Ritchie K (1999) Strength of a weak bond connecting flexible polymer chains. Biophys J 76:2439–2447. doi:10.1016/S0006-3495(99)77399-6

Fabry B, Maksym G, Hubmayr R, Butler J, Fredberg J (1999) Implications of heterogeneous bead behavior on cell mechanical properties measured with magnetic twisting cytometry. J Magn Magn Mater 194:120–125

Fabry B et al (2003) Time scale and other invariants of integrative mechanical behavior in living cells. Phys Rev E Stat Nonlin Soft Matter Phys 68:041914

Féréol S et al (2006) Sensitivity of alveolar macrophages to substrate mechanical and adhesive properties. Cell Motil Cytoskeleton 63:321–340

Féréol S et al (2009) Prestress and adhesion site dynamics control cell sensitivity to extracellular stiffness. Biophys J 96:2009–2022

Féréol S, Fodil R, Pelle G, Louis B, Isabey D (2008) Cell mechanics of alveolar epithelial cells (AECs) and macrophages (AMs). Respir Physiol Neurobiol 163:3–16

Friedl P, Brocker EB (2000) The biology of cell locomotion within three-dimensional extracellular matrix. Cell Mol Life Sci CMLS 57:41–64

Fung YC (ed) (1981) Biomechanics; mechanical properties of living tissues, vol 1. Springer, University of California, San Diego

Gallant ND, Michael KE, Garcia AJ (2005) Cell adhesion strengthening: contributions of adhesive area, integrin binding, and focal adhesion assembly. Mol Biol Cell 16:4329–4340. doi:10.1091/mbc.E05-02-0170

Ingber DE (1997) Integrins, tensegrity, and mechanotransduction. Gravit Space Biol Bull 10:49–55

Isabey D, Féréol S, Caluch A, Fodil R, Louis B, Pelle G (2013) Force distribution on multiple bonds controls the kinetics of adhesion in stretched cells. J Biomech 46:307–313. doi:10.1016/j.jbiomech.2012.10.039

Janmey P (1995) Cell membranes and the cytoskeleton. In: Sackmann RLAE (ed) Handbook of biological physics, vol 1., pp 805-849, Elsevier Science B.V

Jiang H, Grinnell F (2005) Cell-matrix entanglement and mechanical anchorage of fibroblasts in three-dimensional collagen matrices. Mol Biol Cell 16:5070–5076. doi:10.1091/mbc.E05-01-0007

Kokkoli E, Ochsenhirt SE, Tirrell M (2004) Collective and single-molecule interactions of alpha5beta1 integrins. Langmuir 20:2397–2404

Lagunas A, Comelles J, Martinez E, Prats-Alfonso E, Acosta GA, Albericio F, Samitier J (2012) Cell adhesion and focal contact formation on linear RGD molecular gradients: study of non-linear concentration dependence effects. Nanomed Nanotechnol Biol Med 8:432–439. doi:10.1016/j.nano.2011.08.001

Lauffenburger D, Linderman J (1993) Models for binding, trafficking, and signaling. In: Receptors, pp 0-362, Oxford University Press, New York

Laurent VM, Fodil R, Canadas P, Féréol S, Louis B, Planus E, Isabey D (2003) Partitioning of cortical and deep cytoskeleton responses from transient magnetic bead twisting. Ann Biomed Eng 31:1263–1278

Li F, Redick SD, Erickson HP, Moy VT (2003) Force measurements of the alpha5beta1 integrin-fibronectin interaction. Biophys J 84:1252–1262. doi:10.1016/S0006-3495(03)74940-6

Marshall BT, Long M, Piper JW, Yago T, McEver RP, Zhu C (2003) Direct observation of catch bonds involving cell-adhesion molecules. Nature 423:190–193

Matthews BD, Overby DR, Mannix R, Ingber DE (2006) Cellular adaptation to mechanical stress: role of integrins, Rho, cytoskeletal tension and mechanosensitive ion channels. J Cell Sci 119:508–518

Mijailovich SM, Kojic M, Zivkovic M, Fabry B, Fredberg JJ (2002) A finite element model of cell deformation during magnetic bead twisting. J Appl Physiol 93:1429–1436

Miyamoto S, Akiyama SK, Yamada KM (1995) Synergistic roles for receptor occupancy and aggregation in integrin transmembrane function. Science 267:883–885

Mizuno D, Tardin C, Schmidt CF, Mackintosh FC (2007) Nonequilibrium mechanics of active cytoskeletal networks. Science 315:370–373

Na S, Collin O, Chowdhury F, Tay B, Ouyang M, Wang Y, Wang N (2008) Rapid signal transduction in living cells is a unique feature of mechanotransduction. Proc Natl Acad Sci USA 105:6626–6631. doi:10.1073/pnas.0711704105

Noy A, Friddle RW (2013) Practical single molecule force spectroscopy: how to determine fundamental thermodynamic parameters of intermolecular bonds with an atomic force microscope. Methods 60:142–150. doi:10.1016/j.ymeth.2013.03.014

Ohayon J, Tracqui P, Fodil R, Féréol S, Laurent VM, Planus E, Isabey D (2004) Analysis of nonlinear responses of adherent epithelial cells probed by magnetic bead twisting: a finite element model based on a homogenization approach. J Biomech Eng 126:685–698

Pierres A, Benoliel AM, Bongrand P (1996) Measuring bonds between surface-associated molecules. J Immunol Methods 196:105–120

Poh YC, Shevtsov SP, Chowdhury F, Wu DC, Na S, Dundr M, Wang N (2012) Dynamic force-induced direct dissociation of protein complexes in a nuclear body in living cells. Nat Commun 3:866. doi:10.1038/ncomms1873

Pommerenke H, Schreiber E, Durr F, Nebe B, Hahnel C, Moller W, Rychly J (1996) Stimulation of integrin receptors using a magnetic drag force device induces an intracellular free calcium response. Eur J Cell Biol 70:157–164

Potard US, Butler JP, Wang N (1997) Cytoskeletal mechanics in confluent epithelial cells probed through integrins and E-cadherins. Am J Physiol 272:C1654–1663

Ruoslahti E (1996) RGD and other recognition sequences for integrins. Annu Rev Cell Dev Biol 12:697–715. doi:10.1146/annurev.cellbio.12.1.697

Schoen I, Pruitt BL, Vogel V (2013) The Yin-Yang of rigidity sensing: how forces and mechanical properties regulate the cellular response to materials. Ann Rev Mater Res 43:589–618. doi:10.1146/annurev-matsci-062910-100407

Stricker J, Aratyn-Schaus Y, Oakes PW, Gardel ML (2011) Spatiotemporal constraints on the force-dependent growth of focal adhesions. Biophys J 100:2883–2893. doi:10.1016/j.bpj.2011.05.023

Tan JL, Tien J, Pirone DM, Gray DS, Bhadriraju K, Chen CS (2003) Cells lying on a bed of microneedles: an approach to isolate mechanical force. Proc Natl Acad Sci USA 100:1484–1489. doi:10.1073/pnas.0235407100

Trepat X, Grabulosa M, Puig F, Maksym GN, Navajas D, Farré R (2004) Viscoelasticity of human alveolar epithelial cells subjected to stretch. Am J Physiol Lung Cell Mol Physiol 287:L1025–1034

Tsukasaki Y, Kitamura K, Shimizu K, Iwane AH, Takai Y, Yanagida T (2007) Role of multiple bonds between the single cell adhesion molecules, nectin and cadherin, revealed by high sensitive force measurements. J Mol Biol 367:996–1006. doi:10.1016/j.jmb.2006.12.022

Vlahakis NE, Schroeder MA, Limper AH, Hubmayr RD (1999) Stretch induces cytokine release by alveolar epithelial cells in vitro. Am J Physiol 277:L167–173

Wang N, Butler JP, Ingber DE (1993) Mechanotransduction across the cell surface and through the cytoskeleton [see comments]. Science 260:1124–1127

Wendling S, Planus E, Laurent V, Barbe L, Mary A, Oddou C, Isabey D (2000) Role of cellular tone and microenvironmental conditions on cytoskeleton stiffness assessed by tensegrity model. Eur Phys J Appl Phys 9:51–62

Williams PM (2003) Analytical descriptions of dynamic force spectroscopy: behaviour of multiple connections. Anal Chim Acta 479:107–115

Zhang X, Moy VT (2003) Cooperative adhesion of ligand-receptor bonds. Biophys Chem 104:271–278

Zhu C, Bao G, Wang N (2000) Cell mechanics: mechanical response, cell adhesion, and molecular deformation. Annu Rev Biomed Eng 2:189–226. doi:10.1146/annurev.bioeng.2.1.189

Zhu C, Yago T, Lou J, Zarnitsyna VI, McEver RP (2008) Mechanisms for flow-enhanced cell adhesion. Ann Biomed Eng 36:604–621